

Inferring latent structure in ecological communities via barcodes

Braden Scherting¹ and David B. Dunson¹

¹Department of Statistical Science, Duke University

December 13, 2024

Abstract

Accelerating global biodiversity loss has highlighted the role of complex relationships and shared patterns among species in mediating responses to environmental changes. The structure of ecological communities signals their fragility or robustness more so than individual niches of species. We focus on obtaining community-level insights that characterize underlying patterns in abundances of bird species in Finland. We propose a novel `barcode` framework for inferring latent binary features underlying samples and species. `barcode` provides a more nuanced alternative to clustering, while improving current multivariate abundance models. `barcode` addresses key limitations of popular methods for model-based ordination and expands the class of concurrent ordinations. A key feature is our use of binary latent variables, which admit simple interpretations such as habitat and sampling factors that explain observed variation. In studying 137 bird species using this framework, we find that three of the five leading factors indicate different types of forest habitat, signaling the importance of diverse forest in this community. In contrast, a single factor simultaneously proxies both human intervention and coastal habitats. Supervised species clusters and species-specific geospatial distributions are also inferred.

Keywords: Abundance data; Binary latent variables; Clustering; Ecology; Multivariate count data; Ordination.

1 Introduction

Describing, visualizing, and interpreting unobserved sources of variation in multivariate data is of acute importance in studies of large ecological communities. Community data are often represented by large and sparse count matrices. Multivariate count regression can summarize species-specific responses to environmental covariates while characterizing interspecific dependence not explained by covariates. However, in large community settings, parsing covariate effects across hundreds or thousands of species is daunting. Our focus is instead on inferring low-dimensional binary features, underlying samples and species, to provide insights into environmental gradients underlying communities. In addition, we define a new class of multivariate abundance models that improve current multivariate count regression models. Our applied focus is on learning what drives Finnish avian abundances at the community level.

Ecological communities, assemblages of co-occurring and interacting species, underpin all high-functioning ecosystems. Communities arise through the interplay between environmental filtering, interactions between species, and natural stochasticity, which in turn depend on species and habitat traits (Ovaskainen et al., 2017). Global biodiversity loss is a community dynamic and has acute, negative impacts on ecosystem functioning and thus ecosystem services to human populations (Cardinale et al., 2012). The interspecific dependence inherent in ecological communities amplifies biodiversity loss, as extinction events can cascade according to the structure of the community (Ebenman and Jonsson, 2005; Koh et al., 2004). Thus, studying the structure of the community and the processes by which they emerge is essential for effective biomonitoring and conservation.

Birds commonly function as keystone species (Leito et al., 2016) and exhibit strong community effects (Lovette and Hochachka, 2006; Skórka et al., 2014). Ignoring this dependence has practical implications on estimates of responses to climate change (Engelhardt et al.,

2020); conversely, interspecific dependence can also moderate responses to climate change (Ahola et al., 2007). Because birds migrate and/or occupy large ranges, interactions, interspecific dependence, and an intricate community structure are likely. Despite this, many multi-species studies of avian communities restrict their focus to small taxonomic groups or guilds (e.g., Alatalo et al. (1985); Auer and King (2014); Wittwer et al. (2015)). This is effective when the focus is on a few species, but obscures dependencies and fails to borrow information from non-focal species occupying similar niches. Joint species distribution models (JSDM; Warton et al. (2015)) characterize covariate effects on species occurrence, while accounting for residual dependence between species.

However, for moderate to large numbers of species, it is difficult to extract meaningful inferences on community-level dynamics from JSDM results, such as species-level covariate effects. Questions in studying community-level dynamics, such as “*What are key drivers of abundance within the community?*” or “*Which groups of species exhibit similar patterns of occurrence and responses to the environment?*” can be overwhelmed by the sheer number of species-specific inferences. These research questions can be answered more efficiently by models which focus inference on community-level dynamics. Using data on the abundances of 137 avian species endemic to Finland, we investigate the factors responsible for explaining observed variation and infer species latent traits underlying their abundances.

Ordination is a class of multivariate statistical and algorithmic data analysis procedures suited to inference at the community level (Legendre and Legendre, 2012). Most such methods project observed community data onto a lower-dimensional latent space in which visualization, pairwise comparisons of samples and species, and analyses such as clustering and regression are easier to perform. The variation in the learned space represents the environmental gradients that underlie biodiversity. Existing model-based ordination methods struggle to accurately characterize moderate to high-dimensional abundance data. Most of such approaches are based on generalized linear latent variable models (GLLVMs)

that incorporate continuous latent factors in characterizing interspecific dependence.

We instead propose a novel `barcode` framework that relies on binary latent variables within an additive model. This confers several advantages including simplified interpretations of latent factors, structural zero modeling, coherent generalization to out-of-sample settings, and induced sample and species clusters. We demonstrate the statistical imperative and applied relevance of our framework through simulation and the avian community data mentioned above. Before describing our `barcode` approach in detail, we further introduce the motivating data and review relevant modeling competitors.

1.1 Applied setting: Fennoscandian avian communities

National biodiversity monitoring programs are common in many regions and are important tools for informed conservation. Bird monitoring is popular because birds are relatively easy to detect and identify, and they occupy large geographic regions and ecological niches. Fennoscandian bird monitoring surveys have proven valuable in studying declines in mountain species (Lehikoinen et al., 2014) and trends in wader species (Lindström et al., 2015, 2019). To better understand broad trends and borrow information among species groups, we use abundances of 137 species from the Finnish national bird monitoring program documented by Piirainen et al. (2023).

Line transect surveys (sampling units) were conducted by volunteers beginning in 1978. We limit our focus to surveys conducted between 2006 and 2016, as, before 2006, waterbirds were not recorded. This 11 year period includes 2826 surveys at 555 sites; sites were visited between 1 and 11 times each. An average of 260 (1–759) individuals and 38 (1–81) species are recorded in each sample. Species vary widely in recorded abundance; On average, each survey records 40 willow warblers (*Phylloscopus trochilus*; most abundant) and 0.03 ospreys (*Pandion haliaetus*; least abundant). Approximately 72% of the records are zero, and the largest single count is 189 (black-headed gull, *Larus ridibundus*). Sample- and site-specific

auxiliary information is also available. The starting points of the line transects inform the geographic abundance gradients across Finland, and the lengths of the line transects and the duration of the survey serve as proxies for effort. We condition on interpretable covariates, including habitat classifications, forest inventory and volume, and time of year.

Piirainen et al. (2023) modeled the 120 most common species in two stages, first modeling presences and absences using a probit GLLVM and then modeling the logarithm of positive counts using a Gaussian latent variable model. Their analysis was focused exclusively on predicting species abundances at future times rather than interpreting inferred species distributions and environmental gradients.

1.2 Relevant modeling approaches

A principal challenge in ecological community modeling is deciphering patterns of relative abundance among dozens or hundreds of species. Ordination methods assign scores to samples and species based on latent variables. These latent variables are interpreted as environmental gradients or factors that explain the observed variation. Methods for ordination vary in 1) whether or not observed covariates are used to inform/constrain latent variables and 2) whether the latent variables are defined and estimated using a statistical model. Unconstrained ordination is performed without covariates, whereas constrained ordination restricts axes to linear combinations of environmental covariates (Ter Braak and Prentice, 1988). We focus on model-based ordination, which can more flexibly represent properties of biodiversity data, including sparsity and heteroskedasticity, while enabling model checking and uncertainty quantification (Hoegh and Roberts, 2020). Constrained, model-based ordinations generally perform a variation of reduced-rank regression (Davies and Tso, 1982; Yee and Hastie, 2003), whereas unconstrained approaches usually rely on generalized linear latent variable models (Hui et al., 2015).

GLLVMs (Skrondal and Rabe-Hesketh, 2004) are popular in ecology for both ordina-

tion (Hui et al., 2015) and joint species distribution modeling (JSDM) (Niku et al., 2019; Ovaskainen et al., 2017; Tikhonov et al., 2020). Hui (2017); Stratton et al. (2024) use Gaussian mixtures for site scores to infer clusters in an unconstrained ordination approach. To unite advantages of constrained and unconstrained ordination, van der Veen et al. (2023) model site scores as *stochastic* functions of covariates within a GLLVM, an approach they term concurrent ordination.

As JSDMs and model-based ordinations have become siloed within the GLLVM framework, a natural question is whether stepping outside the framework is valuable. Community data are notoriously sparse, especially for diverse communities or large geospatial domains, and abundance counts often vary widely. We show that log-linear specifications underlying Poisson and negative-binomial GLLVMs have poor out-of-sample prediction in the presence of high sparsity and large counts. This manifests as predicting abundances far outside realistic limits.

Our proposed `barcode` approach adopts an additive (instead of multiplicative) mean structure, which helps mitigate extreme nonsensical predictions. Departing from the GLLVM framework affords us the opportunity to introduce different types of latent variables. Recent extensions of latent class models using highly structured and identifiable binary latent variables (Gu and Dunson, 2023; Zhou et al., 2024) showcase the potential of discrete variables to flexibly characterize joint distributions of categorical data. In addition to being intrinsically interpretable, binary latent variables also induce natural clustering without the usual mixture model specification.

In the following, we describe our `barcode` approach to unconstrained and concurrent ordination using a conditionally Poisson additive model and binary latent variables. In simulation studies, `barcode` accurately recovers true latent configurations and generalizes well to unseen data in misspecified settings. We deploy `barcode` to obtain novel community-level insights into Finnish bird populations.

2 Barcode modeling framework

To analyze the avian community described in Sec 1.1, we jointly model the observed abundances of all species using a novel type of Poisson factorization. We model factor scores and factor loadings using a combination of continuous and binary latent variables. Sample-specific binary feature vectors summarize habitat and sampling conditions that are readily interpreted and compared across samples, while species-specific binary vectors describe each species’ preference towards the learned habitat/sampling factors. The discrete latent variables are simple to interpret and exact sparsity automatically disambiguates structural zeros from sampling zeros, an important task in ecological community modeling. Observed covariates and the geographic context are introduced hierarchically to provide interpretations of learned factors. We dub this model **barcode**, **binary** and **real count decomposition**.

For samples $i = 1, 2, \dots, n$ and species $j = 1, 2, \dots, p$, let $y_{ij} \in \{0, 1, 2, \dots\}$ denote the observed abundance of species j in sample i . A sample represents a single line transect survey conducted at one of the $m = 555$ survey sites; the site at which the sample i was collected is denoted by $k_i \in \{1, 2, \dots, m\}$, and the location of the site k_i by \mathbf{s}_{k_i} . Each site was visited between one and eleven times during the study period. Lastly, let $\mathbf{x}_i = (x_{i1}, \dots, x_{iq})^\top$ denote the observed covariates collected for sample i .

2.1 Abundance model

Observed abundances are conditionally Poisson and independent, and the mean is endowed with a factor-analytic structure,

$$(y_{ij} \mid \mu_{ij}) \sim \text{Pois}(\mu_{ij}), \quad \mu_{ij} = \theta_i^\top \lambda_j \geq 0,$$

where $\theta_i = (\theta_{i1}, \dots, \theta_{iL})^\top$ are latent factor scores describing sample i and $\lambda_j = (\lambda_{j1}, \dots, \lambda_{jL})^\top$ are factor loadings, which capture species-specific responses to each of the L factors. Univariate gamma priors on both factor scores and factor loadings yields the Bayesian nonneg-

ative matrix factorization or gamma-Poisson factorization model (Cemgil, 2009; Gopalan et al., 2015). Motivated by improving fit to motivating datasets and the importance of simple-to-interpret, latent structure, `barcode` deviates from gamma-Poisson factorization by introducing *exact* sparsity in factors and loadings,

$$\mu_{ij} = (\mathbf{c}_i \circ \phi_i)^\top (\mathbf{s}_j \circ \gamma_j) = \sum_{l=1}^L (c_{il} \phi_{il}) \times (s_{jl} \gamma_{jl}),$$

where $c_{il} \in \{0, 1\}$ and $s_{jl} \in \{0, 1\}$. Each factor $\theta_{il} = c_{il} \phi_{il}$ is decomposed into a binary “switch” c_{il} and continuous “intensity” ϕ_{il} . Loadings $\lambda_{jl} = s_{jl} \gamma_{jl}$ are decomposed similarly with switch s_{jl} and intensity γ_{jl} . Together, sample factors and species preferences determine the mean: for each l such that $s_{jl} = 1$ **and** $c_{il} = 1$, the expected abundance of species j at the site i increases by $\gamma_{jl} \phi_{il}$, and for each l such that $s_{jl} = 0$ **or** $c_{il} = 0$, the expected abundance is unchanged. Species-specific intensities are assigned a gamma prior,

$$\gamma_{jl} \sim \text{Ga}(a_\gamma, \nu_l), \quad \nu_l \sim \text{Ga}(a_\nu, b_\nu),$$

parameterized such that $\mathbb{E}_{x \sim \text{Ga}(a,b)}[x] = a/b$. To resolve the scale ambiguity between $(\mathbf{c}_l \circ \phi_l)$ and $(\mathbf{s}_l \circ \gamma_l)$, we choose a prior with constrained support.

In particular, following Koslovsky (2023), we define sample intensities through auxiliary variables ζ as

$$\phi_{il} = \frac{\zeta_{il}}{\sum_{i=1}^n \zeta_{il} c_{il}}, \quad \zeta_{il} \sim \text{Ga}(\alpha, 1), \quad (1)$$

which ensures $\mathbf{1}_n^\top (\mathbf{c}_l \circ \phi_l) = 1$. This induces the prior

$$\{\phi_{il} : c_{il} = 1, i = 1, \dots, n\} \sim \text{Dir}(\alpha, \dots, \alpha), \quad (2)$$

which has effective dimension $\sum_i c_{il} \leq N$.

We find that $\alpha = 1$ is a suitable choice in most settings, including the simulations and the case study that we present. Because the scale of factors/loadings is fixed arbitrarily, i.e., $\mathbf{1}_n^\top (\mathbf{c}_l \circ \phi_l) = 1$, ϕ_l scales inversely with n and γ_l . We accommodate this by choosing priors for ν_l that are very flexible and computationally convenient as opposed to informative. We

set $a_\gamma = 0.5$, $a_\nu = 0.5$, and $b_\nu = 0.5$; these do not depend on n , and the marginal expectation and variance of γ are unbounded *a priori*. Additionally, we make no effort to estimate the number of factors, preferring instead to set a manageable value for interpretation (usually 5). When generating marginal species distribution maps, interpreting factors is not the primary objective, so a larger value of L (e.g. 8) is preferred, as it leads to more accurate maps. However, we recognize that there may be settings where automatic or probabilistic selection of the number of factors is desirable; we provide references and additional ideas to this end in Supplement A.

2.2 Priors on factor sparsity

With appropriate priors on $\Pr(c_{il} = 1)$ and $\Pr(s_{jl} = 1)$, the above model performs unconstrained ordination. This is useful for exploratory analysis when few/no covariates are available. We propose using covariates and/or spatial temporal context to aid interpretation of learned factors and study dependence between species abundance and abiotic conditions. Presence/absence of each factor is modeled as a function of covariates and transect location:

$$\Pr(c_{il} = 1) = \begin{cases} 1 & l = 1 \\ \Phi^{-1}(\mathbf{x}_i^\top \beta_l + \xi_l(\mathbf{s}_{k_i})) & l = 2, \dots, L \end{cases} \quad (3)$$

$$\xi_l(\mathbf{s}) \sim \text{GP}(\mathbf{0}, K) \quad \beta_l \sim \text{N}(\mathbf{0}, \sigma_0^2 \mathbf{I}_q)$$

where ξ_l is a smooth, factor-specific spatially-varying intercept, and $\beta_l = (\beta_{l1}, \dots, \beta_{lq})^\top$ characterize the effects of covariates on the presence of factor l . Here, $\mathbf{c}_1 = \mathbf{1}_n$ is the “intercept” and reflects that, in each sample, the conditions were suitable for at least some species to occur and be detected. If the factor intercept is excluded, an arbitrary factor sometimes becomes the *de facto* intercept and estimates of β and ξ become unstable. No such intercept is included in \mathbf{s} , as specialist species may find some sites and samples to be uninhabitable. We let $\Pr(s_{jl} = 1) = \psi \sim \text{Beta}(10, 10)$ *a priori*. We adopt a Gaussian

process for ξ using an exponential covariance with length-scale chosen such that the effective range is approximately equal to the 5% quantile of observed distances. The regression specification can be adapted depending on the context. In simulations studying β recovery and when comparing to other concurrent ordination methods, we exclude ξ . Similarly, when generating marginal species distribution maps, we exclude covariates and β .

2.3 Posterior Computation

We employ a straightforward Gibbs sampler for the posterior computation. Here, we briefly describe the data augmentation strategies used, the sampling procedure, and additional considerations of initialization and tuning.

Additive mean Poisson models are computationally convenient because of the additivity of independent Poisson RVs: the sum of independent Poisson RVs is a Poisson RV. We let

$$y_{ijl} \sim \text{Pois}(c_{il}\phi_{il}s_{jl}\gamma_{jl}), \quad y_{ij} = \sum_{l=1}^L y_{ijl}.$$

Marginally with respect to $\{y_{ijl}\}_{l=1}^L$, this preserves $y_{ij} \sim \text{Pois}(\mu_{ij})$. Then, conditional posteriors for both y_{ijl} and γ_{jl} have simple forms. This augmentation procedure is standard (Dunson and Herring, 2005; Cemgil, 2009; Zhou et al., 2012; Gopalan et al., 2015). Coupled with the fact that $\sum_i c_{il}\phi_{il} = 1$, Poisson additivity additionally implies

$$(y_{1jl}, \dots, y_{njl} \mid -) \sim \text{Mult}\left(y_{\cdot jl}, \left\{ \frac{c_{il}\zeta_{il}}{\sum_{i=1}^n c_{il}\zeta_{il}} \right\}_{i=1}^n\right).$$

Following Koslovsky (2023), this allows us to introduce

$$u_l \sim \text{Ga}\left(\sum_{i,j} y_{ijl}, \sum_i c_{il}\zeta_{il}\right)$$

as a proxy for $\theta_{\cdot l} = \sum_i c_{il}\zeta_{il}$, thus affording simple updates for ζ_{il} . The resulting sampler cycles through the following steps:

1. *Sample binary preferences s_{jl} , $j = 1 : p$ and $l = 1 : L$ from conditionally independent*

posteriors, where

$$\Pr(s_{jl} = 0 | -) \propto \psi \prod_{i=1}^n \left[\mu_{ij}^{(0)} \right]^{y_{ij}} \exp \left[-\mu_{ij}^{(0)} \right], \quad \mu_{ij}^{(0)} = \sum_{l' \neq l} c_{il'} \phi_{il'} s_{jl'} \gamma_{jl'}$$

$$\Pr(s_{jl} = 1 | -) \propto (1 - \psi) \prod_{i=1}^n \left[\mu_{ij}^{(1)} \right]^{y_{ij}} \exp \left[-\mu_{ij}^{(1)} \right], \quad \mu_{ij}^{(1)} = \mu_{ij}^{(0)} + c_{il} \phi_{il} \gamma_{jl}$$

2. Sample binary factors c_{il} , $i = 1 : n$ and $l = 1 : L$ from conditionally independent posteriors, where

$$\Pr(c_{il} = 0 | -) \propto \Phi^{-1} \left(\mathbf{x}_i^\top \beta_l + \xi_{lk_i} \right) \prod_{j=1}^p \left[\mu_{ij}^{(0)} \right]^{y_{ij}} \exp \left[-\mu_{ij}^{(0)} \right],$$

$$\mu_{ij}^{(0)} = \sum_{l' \neq l} c_{il'} \phi_{il'} s_{jl'} \gamma_{jl'}$$

$$\Pr(s_{jl} = 1 | -) \propto \left[1 - \Phi^{-1} \left(\mathbf{x}_i^\top \beta_l + \xi_{lk_i} \right) \right] \psi \prod_{i=1}^n \left[\mu_{ij}^{(1)} \right]^{y_{ij}} \exp \left[-\mu_{ij}^{(1)} \right],$$

$$\mu_{ij}^{(1)} = \mu_{ij}^{(0)} + \phi_{il} s_{jl} \gamma_{jl}$$

3. Sample factor-specific counts $(y_{ij1}, \dots, y_{ijL})$, $i = 1 : n$ and $j = 1 : p$

$$(y_{ij1}, \dots, y_{ijL} | -) \sim \text{Mult}(y_{ij}, \pi_{ij}), \quad \pi_{ijl} = \frac{c_{il} \phi_{il} s_{jl} \gamma_{jl}}{\sum_l c_{il} \phi_{il} s_{jl} \gamma_{jl}}$$

4. Sample preference intensities γ_{jl} , $j = 1 : p$ and $l = 1 : L$:

$$(\gamma_{jl} | -) \sim \text{Ga}(a_\gamma + y_{.jl}, \nu_l + 1)$$

5. Sample auxiliary normalizing constants u_l , $l = 1 : L$:

$$(u_l | -) \sim \text{Ga} \left(y_{\cdot l}, \sum_i c_{il} \zeta_{il} \right)$$

6. Sample unnormalized factor intensities ζ_{il} , $i = 1 : n$ and $l = 1 : L$:

$$(\zeta_{il} | -) \sim \text{Ga}(\alpha + y_{i\cdot l}, 1 + u_l)$$

7. Sample latent regression coefficients and random effects β , ξ following Albert and Chib (1993).

8. *Sample hyperparameters ψ and $\nu_l, l = 1 : L$ from conditionally independent posteriors.*

The sampler is generally efficient. We employ three simple strategies to further improve efficiency: (1) a pseudo-prior for γ_{jl} , (2) jointly updating blocks of binary latent variables to encourage exploration of discrete space, and 3) a warm start to limit the influence of multimodality inherent to Poisson factorization models. These strategies are detailed further in Supplement B.

2.4 Properties of barcode

`barcode` performs unconstrained and concurrent ordination, accommodates extreme sparsity, disambiguates random and structural zeros, clusters samples by habitat profile and species by habitat preference, and produces accurate predictions. Here, we provide more detail on the role of binary latent variables in modeling zeros and clustering.

Sparsity & structural zeros: Zero counts are common in community data and may be due to true absence, sampling error, or basic randomness (Blasco-Moreno et al., 2019). The latent binary skeleton of `barcode`, $\mathbf{c}_i^\top \mathbf{s}_j$, disambiguates zeros that occur with probability less than 1 (random) from those occurring with probability 1 (structural). The skeleton is the inner product between sample-specific \mathbf{c}_i and species-specific \mathbf{s}_j , and provides an integer score, $\mathbf{c}_i^\top \mathbf{s}_j \in \{0, 1, \dots, L\}$. The skeleton score $\mathbf{c}_i^\top \mathbf{s}_j = 0$ when no factors required by species j are in sample i . Then, $\Pr(y_{ij} = 0 \mid \mathbf{c}_i^\top \mathbf{s}_j = 0) = 1$, as $\mathbf{c}_i^\top \mathbf{s}_j = 0 \implies \mu_{ij} = 0$, while $\Pr(y_{ij} = 0 \mid \mathbf{c}_i^\top \mathbf{s}_j > 0) > 0$. The posterior probability of a structural zero, $\Pr(\mathbf{c}_i^\top \mathbf{s}_j = 0 \mid \mathbf{Y})$, can be estimated directly from the MCMC samples.

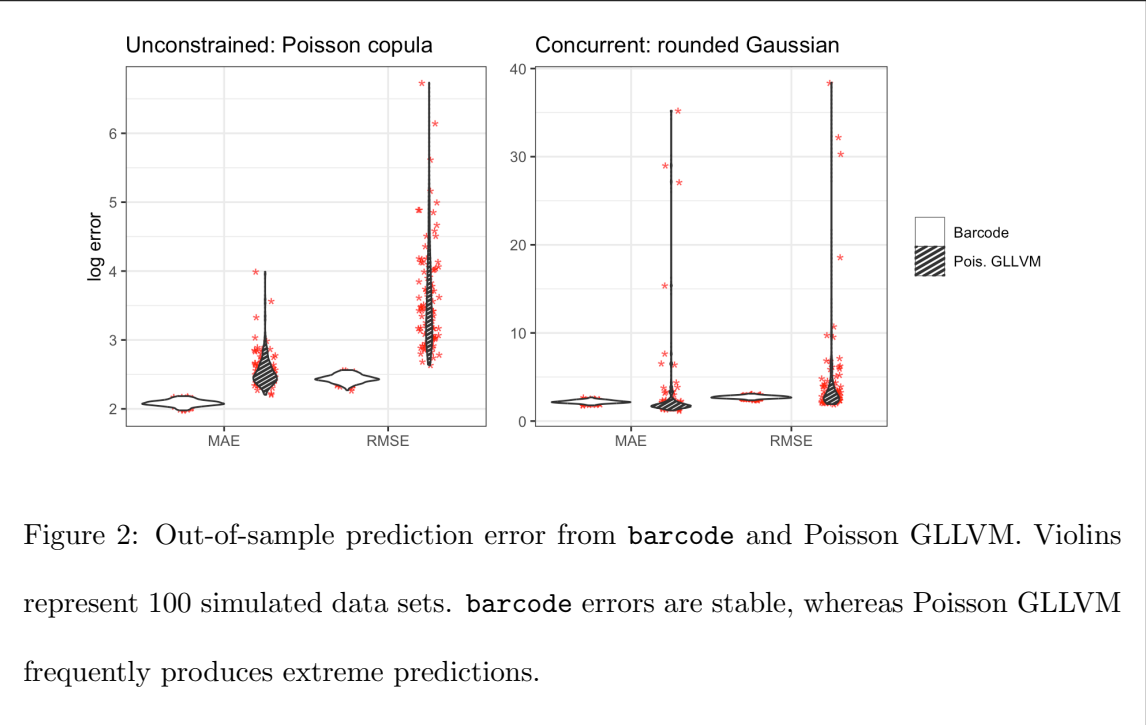
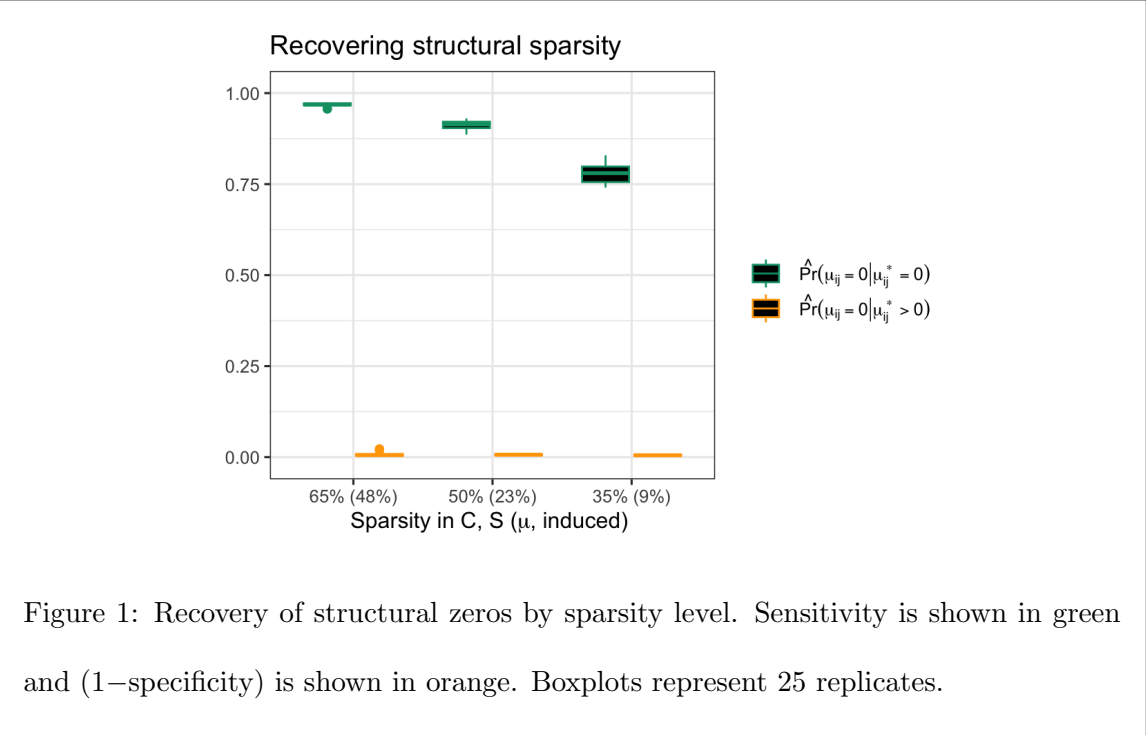
Clustering: `barcode` incorporates binary sample- and species-specific latent variables within a generative probability model for the multivariate abundance counts. We use these latent variables for inferences as a more nuanced alternative to clustering. In addition, we can infer clusters of samples and species according to groups having identical binary traits.

3 Simulation Study

We investigated the performance of `barcode` through simulation to certify the model’s ability to recover 1) sparse expectations (structural zeros), 2) sparse latent variables, and 3) latent regression coefficients that control/explain latent variables. Subsequently, we evaluate fit to data under model misspecification and compare to unconstrained and concurrent GLLVMs.

The first set of simulations evaluates the recovery of latent parameters when the model is correctly specified, starting with structural sparsity (i.e., $\mu_{ij} = 0$). We generate data from the unconstrained (static) `barcode` model with 3 different levels of sparsity in C and S : 35%, 50% and 65%; two $L \times L$ identity blocks are included in S . These latent configurations induce 9%, 23%, and 48% sparsity in $M = [\mu_{ij}]$. For each sparsity level, we generate 25 data sets by first simulating Φ and Γ from $\text{Ga}(1, \frac{1}{3})$ and $\text{Ga}(1, \frac{1}{5})$, respectively, and finally simulating Y element-wise from the appropriate conditional Poisson distribution. The generating distributions used for Φ and Γ are chosen to have a large variance to induce very large and very small non-zero values in M . The nonstructural zeros in Y (that is, $\{(i, j) : y_{ij} = 0, \mu_{ij} > 0\}$) account for 10% - 40% of the total zeros depending on the level of sparsity in C and S . The true values of Φ and Γ are not recoverable, as we arbitrarily constrain Φ in model fitting. For this experiment, we set $n = 250$, $p = 50$, and $L = 5$.

After fitting the model with default settings, we examine two quantities from each configuration: 1) the average posterior probability of $\mu_{ij} = 0$ across i, j such that $\mu_{ij}^{sim} = 0$ and 2) the average posterior probability of $\mu_{ij} = 0$ across i, j such that $\mu_{ij}^{sim} > 0$ (Fig. 1). We note that the latter quantity, the probability of misidentifying a positive expectation as zero, is only possible in the case $y_{ij} = 0$. The result suggests that structural zeros can be reliably identified from sparse counts when both sparse and small expectations are involved, recovery is best when Y is more sparse, and $\Pr(\mu_{ij} = 0 \mid -) > 0.75$ is a good classification



rule for structural zeros.

Next, we evaluate recovery of the binary latent variables C and S . For $n = (100, 250, 500)$ and $p = 30$, we generate C and S , ensuring that no rows of C or S are all zero (that is, no rows or columns of Y are deterministically zero), and simulate Φ , Γ and Y as above. Furthermore, for $p = (15, 30, 50)$ and $n = 250$ we perform the same procedure. This is repeated 25 times for each (n, p) . Varying n affects the effective sample size for estimating s_j and varying p affects the effective sample size for estimating c_i . We do not observe label switching, but must permute columns of \hat{C} and \hat{S} to make direct comparisons. The permutation that minimizes the mean absolute difference is used (Fig. 3, a,b). Recovery improves reliably with an effective sample size.

We additionally simulate under the concurrent **barcode** model (i.e, Eq. 3), varying $n = (100, 250, 500, 1000)$, to confirm that latent effects on factor presence are recoverable. For each n , 25 data sets are simulated. The results are shown in Figure 3 c. Posterior credible intervals reliably cover the true value and narrow as n increases. Figure 3 displays estimates of B for one of the 25 data sets. The results of these simulations are somewhat unsurprising: the correctly specified model reliably recovers data-generating parameters. However, this reveals an attractive property of discrete latent variables: S and C are identifiable up to permutation. Evidently, rotational invariance does not complicate interpreting latent factors. In the context of recent theoretical developments on identifiability in a wide range of latent class models (Gu and Dunson, 2023; Lee and Gu, 2024), this is also unsurprising.

The second suite of simulations is designed to evaluate model performance in more realistic settings and compare with the leading competitor. To do so, we simulate from two different data generating processes: 1) Poisson copula with low rank correlation, and 2) rounded linear Gaussian factor model with factors depending on simulated covariates. The unconstrained **barcode** and Poisson GLLVM (PoGLLVM) were fit to the data of

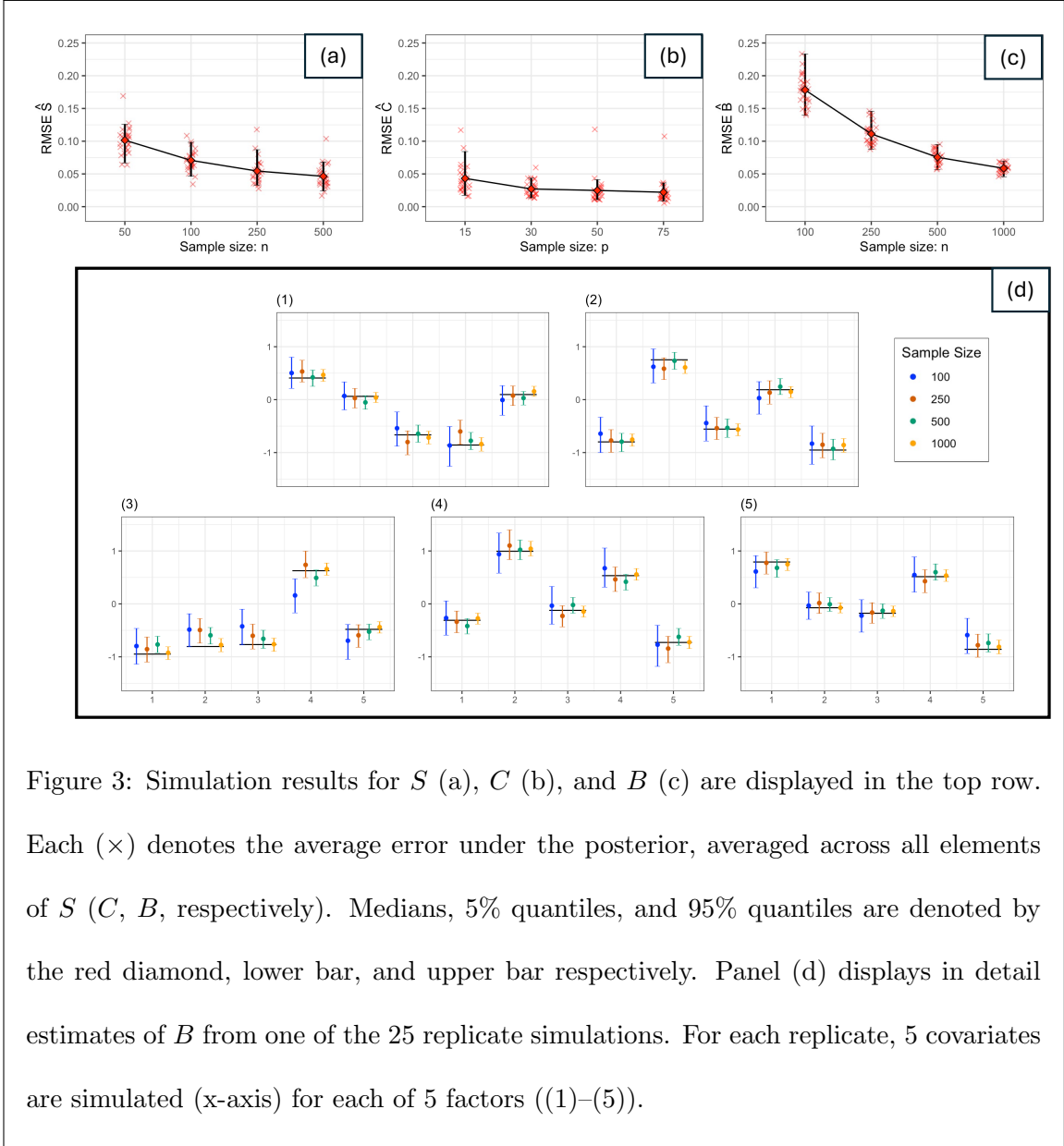
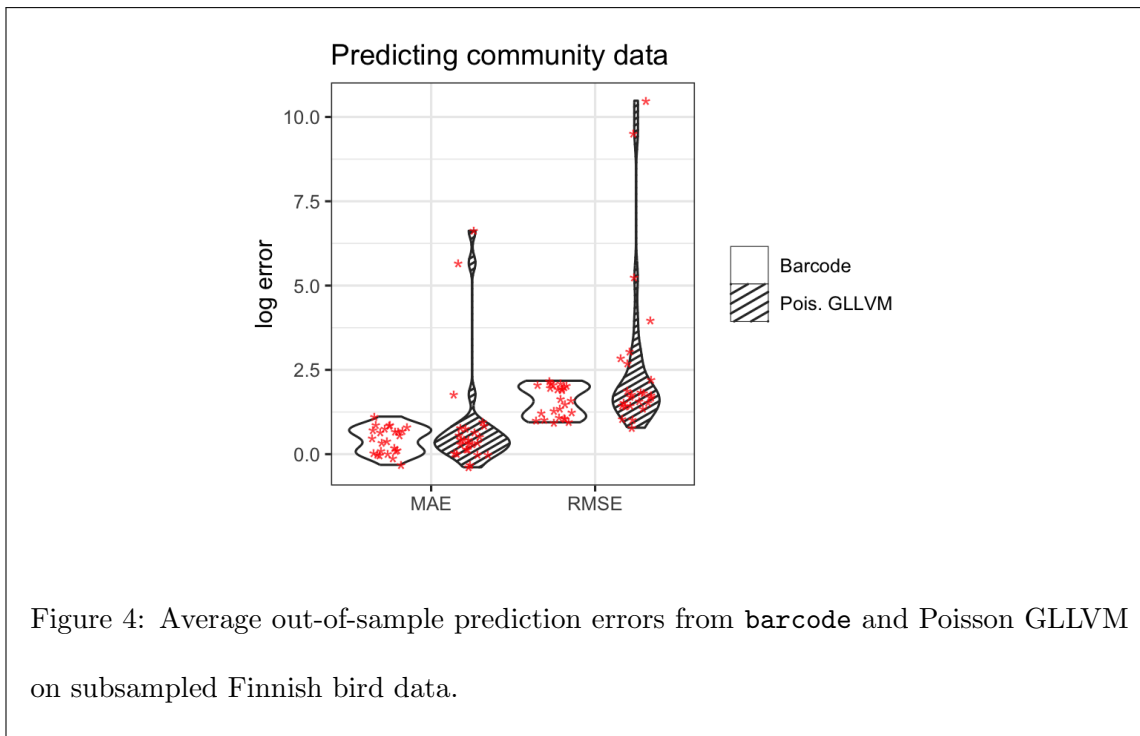


Figure 3: Simulation results for S (a), C (b), and B (c) are displayed in the top row. Each (\times) denotes the average error under the posterior, averaged across all elements of S (C , B , respectively). Medians, 5% quantiles, and 95% quantiles are denoted by the red diamond, lower bar, and upper bar respectively. Panel (d) displays in detail estimates of B from one of the 25 replicate simulations. For each replicate, 5 covariates are simulated (x-axis) for each of 5 factors ((1)–(5)).

process (1), and concurrent versions of each were fit to the data of process (2). Thus, in all simulations, both models are misspecified. Negative binomial GLLVM was also considered, but the prediction error was consistently many orders of magnitude larger than other approaches, so the results are excluded. For each process, 100 data sets were simulated and the models were fit to 80% of observations; we then predicted the held-out 20%. The out-of-sample prediction error is chosen to compare the results, as direct comparison of the inferred parameters is not possible. The results are summarized in Figures 2. In an unconstrained environment, **barcode** consistently outperforms PoGLLVM. PoGLLVM often predicts many of the heldout data accurately, but consistently gives extreme predictions for some. In the concurrent setting, **barcode** performs consistently, whereas PoGLLVM sometimes predicts better and sometimes gives predictions far outside sensible ranges. Prediction is a routine task in ecology, and predictive accuracy reflects the degree to which the model is learning underlying structural patterns in the data.

4 Results for Finnish Bird Abundance Data

We now present the results of applying the **barcode** framework to the abundance data introduced in Sec. 1.1. We study three forms of insights provided by the model: 1) the identities of factors driving abundance, 2) species-specific distributions, and 3) interspecific dependence. A simple experiment confirms that the catastrophic GLLVM prediction behavior observed in simulated settings persists in this case. We subsampled 25 data sets ($n = 300$, $p = 30$), holding out 25% for prediction and fit **barcode** and Poisson GLLVM models. Figure 4 displays the resulting prediction errors. **barcode** gives stable, sensible predictions, while Poisson GLLVM sporadically predicts extreme values.



4.1 Factors driving Finnish avian abundance

We first fit the model to all data using an intercept and five free factors. Each factor is present in (100%, 40%, 34%, 18%, 69%, 62%) of the samples, respectively, and (27%, 73%, 58%, 34%, 67%, 74%) percent of species load on each corresponding factor. Only 27% species load on the intercept and thus have positive expectation in all samples. This set of 36 “generalist” species is diverse both in terms of traits and relative abundance and includes the short-eared owl (*Asio Flammeus*), common snipe (*Gallinago gallinago*), and gray-headed chickadee (*Poecile cinctus*). Zeros make up 72% of the observations; we estimate that only 12.5% of these are structural (y_{ij} is declared a structural zero if $\widehat{\Pr}(\mu_{ij} = 0 \mid \text{—}) > 0.75$). Estimates of structural zeros are generally unambiguous in the following sense: 95% of expected values are positive with probability > 0.75 or zero with probability > 0.75 . However, no expected values are zero with probability ≈ 1 , while 80% of expected values are positive with probability ≈ 1 .

Figure 5 displays the distributions of nonconstant factors on the map of Finland. The

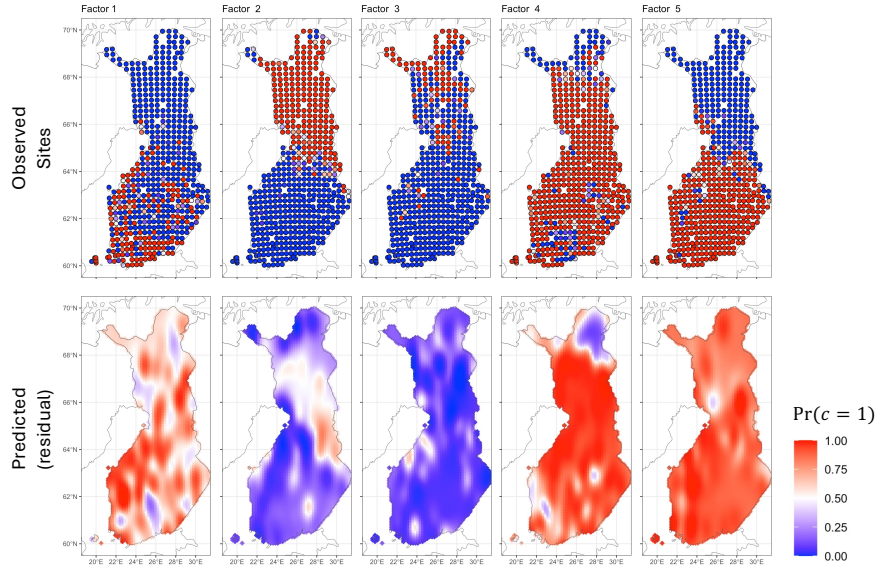


Figure 5: Site-specific factor presences, averaged over samples (top row), and residual predictions across the study area (bottom row).

points in the first row of the maps indicate the presence of the factors in the sites, averaged over the samples taken at each site. Most factors are constant within sites. Spatial variation in factor distributions is due to a combination of spatially varying covariates and residual autocorrelation, as can be seen by comparing top and bottom rows of Figure 5. Among the geographic patterns, the most striking is the latitudinal divide at 65° N in factors 2 and 5. Factors 2 and 5 are largely non-overlapping. The latitudinal gradient displayed by factor 5 is principally due to covariate effects, as evidenced by the constancy of the residuals.

Figure 6 provides a more precise characterization of the environmental niches represented by each factor. Factor interpretations should be made carefully, as patterns in latent factor occurrence are due to both observed and unobserved environmental gradients. We first interpret factors directly based on covariate effects. However, as noted in the following, learned clusters can help refine these interpretations. Factor 1 proxies human intervention: the agricultural and urban settings increase and the density of the forest de-

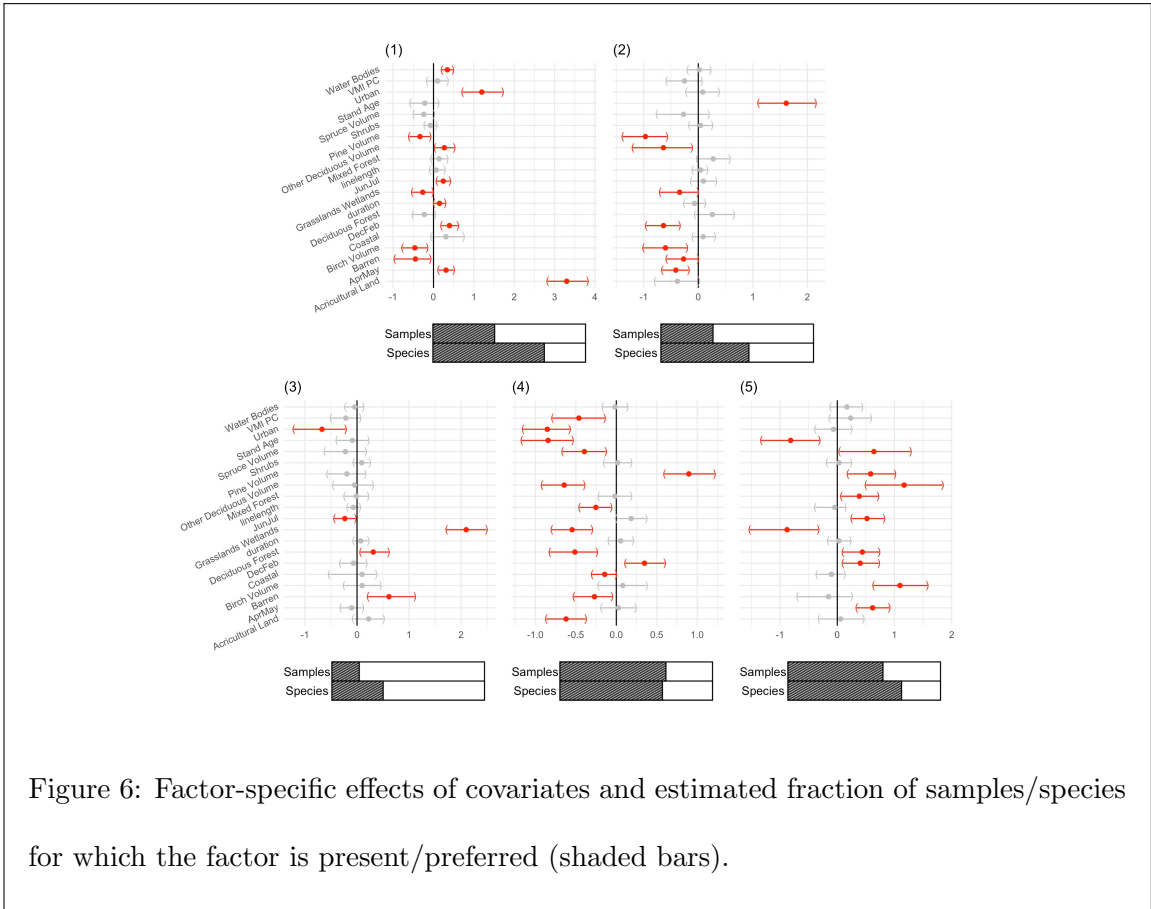


Figure 6: Factor-specific effects of covariates and estimated fraction of samples/species for which the factor is present/preferred (shaded bars).

creases the probability of this factor. This interpretation is consistent with the patterns made in Figure 5; the presence of factor 1 corresponds to regions of high population density. Factors 2 and 5 exhibit opposite trends in terms of covariate effects: factor 2 is associated with low-density, old-growth forests, whereas factor 5 occurs in regions with young, dense wood. The marginal occurrences of factors 2 and 5 are also strongly negatively correlated. Open areas, including grasslands, wetlands, and tundra that are removed from urban areas, beget factor 3. This is the least prevalent factor in terms of both occurrence in samples and preference by species. Factor 4 is highly prevalent and indicates that pine forest environments are specialists. The learned factors appear to be driven by the environmental characteristics of the samples rather than the intensity of the sampling: the effects of both line length and duration on all factors are null or very small relative to other effects. The fact that three of the five leading factors all correspond to forest composition is interesting and suggests that *diversity* in forest composition is extremely important for understanding patterns of avian abundance: not all forests are the same and their differences are key.

4.2 Community distributions

Induced species clusters reveal some interesting patterns. Species cluster assignments are based on the entry-wise median of S . Of the 63 ($2^L - 1$) candidate species clusters, 35 are occupied, and 12 are occupied by only one species. The five most populous groups account for 45% of species, and all five of those clusters share a preference for factor 5, young and diverse forests. The four leading clusters also share preferences for factor 1, agricultural/urban. Clusters which have only one active factor (e.g., 001000 or 000001) should be occupied by specialist species; when the factor is not present, specialist abundance is zero with probability one. The urban-specialist cluster is occupied by six species: common pigeon (*Columba livia*), house sparrow (*Passer domesticus*), mute swan (*Cygnus olor*), common starling (*Sturnus vulgaris*), European goldfinch (*Carduelis carduelis*), and

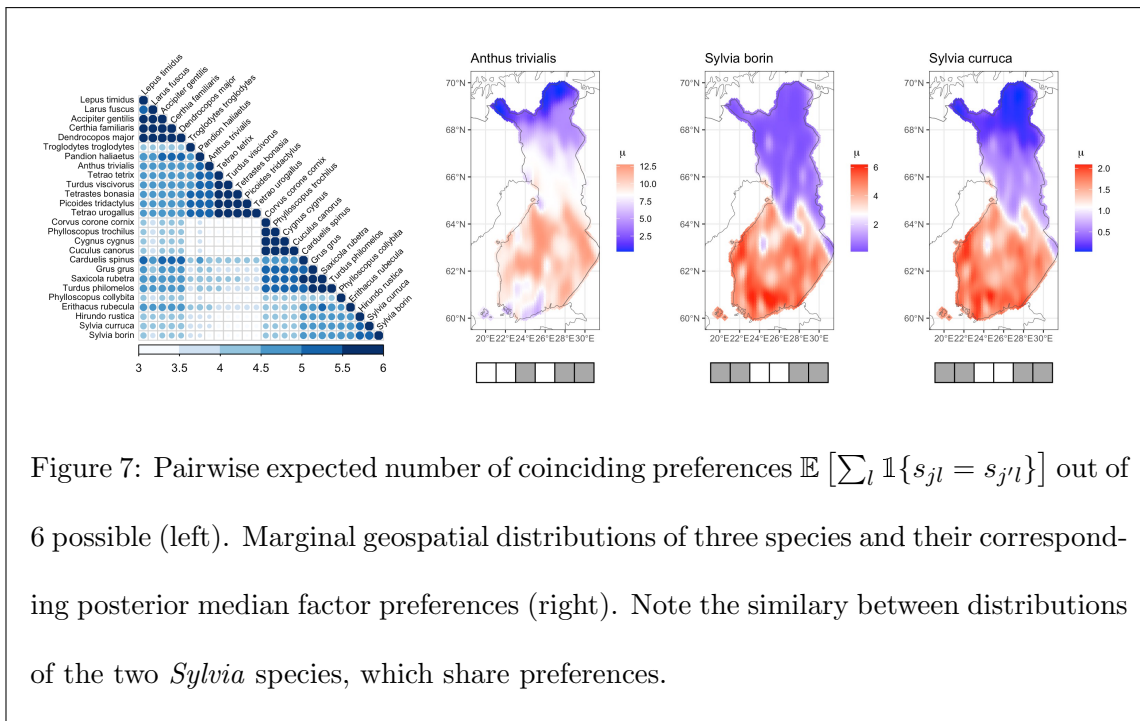


Figure 7: Pairwise expected number of coinciding preferences $\mathbb{E} [\sum_l \mathbb{1}\{s_{jl} = s_{j'l}\}]$ out of 6 possible (left). Marginal geospatial distributions of three species and their corresponding posterior median factor preferences (right). Note the similarity between distributions of the two *Sylvia* species, which share preferences.

Eurasian oystercatcher (*Haematopus ostralegus*). This assemblage largely supports the interpretation of factor 1 as urban/agricultural. However, the presence of the Eurasian oystercatcher in this specialist cluster alerts us that the “urban” factor may be confounded with coastal environments, as the oystercatcher is a wader species and a good deal of Finnish urban areas lie along the coast. This exemplifies the complementary roles of the latent regression and clustering in the **barcode** framework, and highlights that factors can reflect both observed and unobserved environmental gradients. Clusters are useful for explicitly grouping species (or samples), but they also exhibit smoothness in the following basic sense: 110010 is more similar to 100010 than to 001101. An alternative summary of interspecific dependence is based on the *number* of species’ corresponding preferences

$$\Delta_{jj'} = \sum_l \mathbb{1}\{s_{jl} = s_{j'l}\}.$$

Naturally, this count of preference agreements can be summarized probabilistically from MCMC samples and gives a smoother summary of dependence and similarity among species. Figure 7 displays similarities among a subset of species. We include marginal spatial distri-

bution maps of the three species, two typical warblers (genus *Sylvia*) and one pipit (*Anthus*). Marginal species distribution maps are obtained by fitting `barcode` with 8 factors and no covariates (i.e., unconstrained with smooth, site random effects for $\Pr(c_{il} = 1)$). Thus, species distribution maps are superimposed factor maps scaled by species preferences and intensities. The two highlighted warblers both belong to cluster 110011, and their marginal distributions are thus very similar. Though not obvious from either the cluster assignment or the species maps, the Δ -scores indicate that the tree pipit shares more preferences with the lesser whitethroat (*Sylvia curruca*) than with the garden warbler (*Sylvia borin*).

5 Discussion

We introduced an approach to unconstrained and concurrent ordination that utilizes an additive Poisson model and discrete latent variables to learn interpretable factors driving variation in observed abundance data. The model structure enables community-level inference through simultaneous ordination, clustering, and latent regression. We found that log-linear models often generalize poorly to unseen data compared to our proposed approach; the use of discrete latent variables in additive models generalize far better and enable a wide variety of interpretable inferences. Application to Finnish avian community data revealed that diversity in the forest type is responsible for most of the variation we observe and that the community can be partitioned effectively based on habitat preferences.

This analysis expands the suite of models useful for ordination and clustering using abundance data. Although the development of this approach is motivated in part by deficiencies of existing multivariate count models, extending to presence/absence data would be both straightforward and useful. A popular strategy for modeling binary data without the usual logit or probit transformations is to threshold a latent count (Dunson and Herring, 2005). This simple modification to `barcode` would yield a flexible model for co-occurrence

data that retains many of the same interpretations. Given the close relationship between JSDMs and ordination, we also hope to see further development of JSDMs using additive or approximately linear mean structures in the future.

References

- M. P. Ahola, T. Laaksonen, T. Eeva, and E. Lehikoinen. Climate change can alter competitive relationships between resident and migratory birds. *Journal of Animal Ecology*, 76(6):1045–1052, 2007.
- R. V. Alatalo, L. Gustafsson, A. Lundberg, and S. Ulfstrand. Habitat shift of the Willow Tit *Parus montanus* in the absence of the Marsh Tit *Parus palustris*. *Ornis Scandinavica*, 16(2):121–128, 1985.
- J. H. Albert and S. Chib. Bayesian analysis of binary and polychotomous response data. *Journal of the American Statistical Association*, 88(422):669–679, 1993.
- S. K. Auer and D. I. King. Ecological and life-history traits explain recent boundary shifts in elevation and latitude of western North American songbirds. *Global Ecology and Biogeography*, 23(8):867–875, 2014.
- A. Blasco-Moreno, M. Pérez-Casany, P. Puig, M. Morante, and E. Castells. What does a zero mean? Understanding false, random and structural zeros in ecology. *Methods in Ecology and Evolution*, 10(7):949–959, 2019.
- B. J. Cardinale, J. E. Duffy, A. Gonzalez, D. U. Hooper, C. Perrings, P. Venail, A. Narwani, G. M. Mace, D. Tilman, D. A. Wardle, et al. Biodiversity loss and its impact on humanity. *Nature*, 486(7401):59–67, 2012.
- C. M. Carvalho, J. Chang, J. E. Lucas, J. R. Nevins, Q. Wang, and M. West. High-

- dimensional sparse factor modeling: applications in gene expression genomics. *Journal of the American Statistical Association*, 103(484):1438–1456, 2008.
- A. T. Cemgil. Bayesian inference for nonnegative matrix factorisation models. *Computational Intelligence and Neuroscience*, 2009(1):785152, 2009.
- P. Davies and M. K. Tso. Procedures for reduced-rank regression. *Journal of the Royal Statistical Society Series C: Applied Statistics*, 31(3):244–255, 1982.
- P. Dellaportas, J. J. Forster, and I. Ntzoufras. On Bayesian model and variable selection using MCMC. *Statistics and Computing*, 12(1):27–36, 2002.
- D. B. Dunson and A. H. Herring. Bayesian latent variable models for mixed discrete outcomes. *Biostatistics*, 6(1):11–25, 2005.
- B. Ebenman and T. Jonsson. Using community viability analysis to identify fragile systems and keystone species. *Trends in Ecology & Evolution*, 20(10):568–575, 2005.
- E. K. Engelhardt, E. L. Neuschulz, and C. Hof. Ignoring biotic interactions overestimates climate change effects: The potential response of the spotted nutcracker to changes in climate and resource plants. *Journal of Biogeography*, 47(1):143–154, 2020.
- S. Frühwirth-Schnatter. Generalized cumulative shrinkage process priors with applications to sparse bayesian factor analysis. *Philosophical Transactions of the Royal Society A*, 381(2247):20220148, 2023.
- R. Gaujoux and C. Seoighe. A flexible R package for nonnegative matrix factorization. *BMC Bioinformatics*, 11:1–9, 2010.
- A. Gelman and D. B. Rubin. Inference from iterative simulation using multiple sequences. *Statistical science*, 7(4):457–472, 1992.

- P. Gopalan, J. M. Hofman, and D. M. Blei. Scalable recommendation with hierarchical poisson factorization. In *UAI*, pages 326–335, 2015.
- Y. Gu and D. B. Dunson. Bayesian pyramids: Identifiable multilayer discrete latent structure models for discrete data. *Journal of the Royal Statistical Society Series B: Statistical Methodology*, 85(2):399–426, 2023.
- A. Hoegh and D. W. Roberts. Evaluating and presenting uncertainty in model-based unconstrained ordination. *Ecology and Evolution*, 10(1):59–69, 2020.
- F. K. Hui. Model-based simultaneous clustering and ordination of multivariate abundance data in ecology. *Computational Statistics & Data Analysis*, 105:1–10, 2017.
- F. K. Hui, S. Taskinen, S. Pledger, S. D. Foster, and D. I. Warton. Model-based approaches to unconstrained ordination. *Methods in Ecology and Evolution*, 6(4):399–411, 2015.
- L. P. Koh, R. R. Dunn, N. S. Sodhi, R. K. Colwell, H. C. Proctor, and V. S. Smith. Species coextinctions and the biodiversity crisis. *Science*, 305(5690):1632–1634, 2004.
- M. D. Koslovsky. A Bayesian zero-inflated Dirichlet-multinomial regression model for multivariate compositional count data. *Biometrics*, 79(4):3239–3251, 2023.
- A. Lal, K. Liu, R. Tibshirani, A. Sidow, and D. Ramazzotti. De novo mutational signature discovery in tumor genomes using sparsesignatures. *PLoS computational biology*, 17(6):e1009119, 2021.
- S. Lee and Y. Gu. New paradigm of identifiable general-response cognitive diagnostic models: beyond categorical data. *Psychometrika*, 89:1–33, 2024.
- P. Legendre and L. Legendre. *Numerical ecology*. Elsevier, 2012.
- S. Legramanti, D. Durante, and D. B. Dunson. Bayesian cumulative shrinkage for infinite factorizations. *Biometrika*, 107(3):745–752, 2020.

- A. Lehikoinen, M. Green, M. Husby, J. A. Kålås, and Å. Lindström. Common montane birds are declining in northern Europe. *Journal of Avian Biology*, 45(1):3–14, 2014.
- A. Leito, M. Leivits, A. Leivits, J. Raet, R. Ward, I. Ott, H. Tullus, R. Rosenvald, K. Kimmel, and K. Sepp. Black-headed gull (*larus ridibundus* l.) as a keystone species in the lake bird community in primary forest-mire-lake ecosystem. *Baltic Forestry*, 22(1):34–45, 2016.
- Å. Lindström, M. Green, M. Husby, J. A. Kålås, and A. Lehikoinen. Large-scale monitoring of waders on their boreal and arctic breeding grounds in northern Europe. *Ardea*, 103(1):3–15, 2015.
- Å. Lindström, M. Green, M. Husby, J. A. Kålås, A. Lehikoinen, M. Stjernman, et al. Population trends of waders on their boreal and arctic breeding grounds in northern Europe. *Wader Study*, 126(3):200–216, 2019.
- I. J. Lovette and W. M. Hochachka. Simultaneous effects of phylogenetic niche conservatism and competition on avian community structure. *Ecology*, 87(sp7):S14–S28, 2006.
- E. C. Merkle, D. Furr, and S. Rabe-Hesketh. Bayesian comparison of latent variable models: Conditional versus marginal likelihoods. *Psychometrika*, 84:802–829, 2019.
- J. Niku, F. K. Hui, S. Taskinen, and D. I. Warton. `gllvm`: Fast analysis of multivariate abundance data with generalized linear latent variable models in R. *Methods in Ecology and Evolution*, 10(12):2173–2182, 2019.
- O. Ovaskainen, G. Tikhonov, A. Norberg, F. Guillaume Blanchet, L. Duan, D. Dunson, T. Roslin, and N. Abrego. How to make more out of community data? a conceptual framework and its implementation as models and software. *Ecology Letters*, 20(5):561–576, 2017.

- S. Piirainen, A. Lehtikoinen, M. Husby, J. A. Kålås, Å. Lindström, and O. Ovaskainen. Species distributions models may predict accurately future distributions but poorly how distributions change: A critical perspective on model validation. *Diversity and Distributions*, 29(5):654–665, 2023.
- P. Skórka, R. Martyka, J. D. Wójcik, and M. Lenda. An invasive gull displaces native waterbirds to breeding habitats more exposed to native predators. *Population Ecology*, 56:359–374, 2014.
- A. Skrondal and S. Rabe-Hesketh. *Generalized latent variable modeling: Multilevel, longitudinal, and structural equation models*. Chapman and Hall/CRC, 2004.
- C. Stratton, A. Hoegh, T. J. Rodhouse, J. L. Green, K. M. Banner, and K. M. Irvine. Clustering and unconstrained ordination with dirichlet process mixture models. *Methods in Ecology and Evolution*, 15(9):1720–1732, 2024.
- C. J. Ter Braak and I. C. Prentice. A theory of gradient analysis. *Advances in Ecological Research*, 18:271–317, 1988.
- G. Tikhonov, Ø. H. Opedal, N. Abrego, A. Lehtikoinen, M. M. de Jonge, J. Oksanen, and O. Ovaskainen. Joint species distribution modelling with the R-package Hmsc. *Methods in Ecology and Evolution*, 11(3):442–447, 2020.
- B. van der Veen, F. K. Hui, K. A. Hovstad, and R. B. O’Hara. Concurrent ordination: Simultaneous unconstrained and constrained latent variable modelling. *Methods in Ecology and Evolution*, 14(2):683–695, 2023.
- A. Vehtari, A. Gelman, and J. Gabry. Practical bayesian model evaluation using leave-one-out cross-validation and waic. *Statistics and computing*, 27:1413–1432, 2017.
- D. I. Warton, F. G. Blanchet, R. B. O’Hara, O. Ovaskainen, S. Taskinen, S. C. Walker, and

- F. K. Hui. So many variables: joint modeling in community ecology. *Trends in Ecology & Evolution*, 30(12):766–779, 2015.
- T. Wittwer, R. B. O’Hara, P. Caplat, T. Hickler, and H. G. Smith. Long-term population dynamics of a migrant bird suggests interaction of climate change and competition with resident species. *Oikos*, 124(9):1151–1159, 2015.
- T. W. Yee and T. J. Hastie. Reduced-rank vector generalized linear models. *Statistical Modelling*, 3(1):15–41, 2003.
- M. Zhou, L. Hannah, D. Dunson, and L. Carin. Beta-negative binomial process and poisson factor analysis. In N. D. Lawrence and M. Girolami, editors, *Proceedings of the Fifteenth International Conference on Artificial Intelligence and Statistics*, volume 22 of *Proceedings of Machine Learning Research*, pages 1462–1471, La Palma, Canary Islands, 21–23 Apr 2012. PMLR. URL <https://proceedings.mlr.press/v22/zhou12c.html>.
- Y. Zhou, Y. Gu, and D. B. Dunson. Bayesian deep generative models for replicated networks with multiscale overlapping clusters. *arXiv preprint arXiv:2405.20936*, 2024.
- A. Zito and J. W. Miller. Compressive Bayesian non-negative matrix factorization for mutational signatures analysis. *arXiv preprint arXiv:2404.10974*, 2024.

Acknowledgments

This research was partially supported by the National Institutes of Health (grant ID R01ES035625), by the European Research Council under the European Union’s Horizon 2020 research and innovation programme (grant agreement No 856506), and by the Office of Naval Research (N00014-21-1-2510; N00014-24-1-2626). The authors thank Otso Ovaskainen and the Lifeplan team for providing data and helpful comments.

Code Availability

Code available at <https://github.com/braden-scherting/barcode>

Supplementary Materials

A Selecting the number of factors L

The factorization rank L can be chosen to facilitate interpretation, set based on information criteria/fit to data, or estimated as part of an expanded joint model. WAIC is a good choice for comparing Bayesian latent factors models with different factorization ranks, because it can be readily computed, does not directly depend on the number of model parameters, and approximates out-of-sample prediction accuracy; see Merkle et al. (2019) for details and discussion of its use in different practical settings, and Vehtari et al. (2017) for computational considerations. For a prediction-based approach tailored to nonnegative matrix factorization that employs regularization and cross-validation directly, see Lal et al. (2021). Analogous regularization could be applied through a prior. For both WAIC and cross-validation, the model must be refit for each level of regularization and/or factorization rank. This can be avoided by using a hyperprior that controls shrinkage and the number of factors directly.

Estimating the number of latent factors in Gaussian factor models using shrinkage priors has received considerable attention (Carvalho et al., 2008; Legramanti et al., 2020; Frühwirth-Schnatter, 2023). Zito and Miller (2024) develop an approach tailored to the Poisson factorization model using a compressive hyperprior that shrinks the factor loadings matrix column-wise. Adopting this prior for Γ would be natural, as Zito and Miller (2024) use the same factor/loading scale. The matrix S would indirectly induce partial sparsity in redundant factors. To achieve exact column-wise sparsity, S could be thresholded based on corresponding values of Γ - e.g., if $\gamma_{jl} < \epsilon$, $s_{jl} = 0$. The threshold could also be applied

to entire columns based on the estimated relevance weights under their compressive prior framework. Alternatively, factor-specific preference probabilities $\{\psi_l\}$ could be introduced and appropriate shrinkage priors assigned to induce sparsity directly through S , an approach related to spike-and-slab priors.

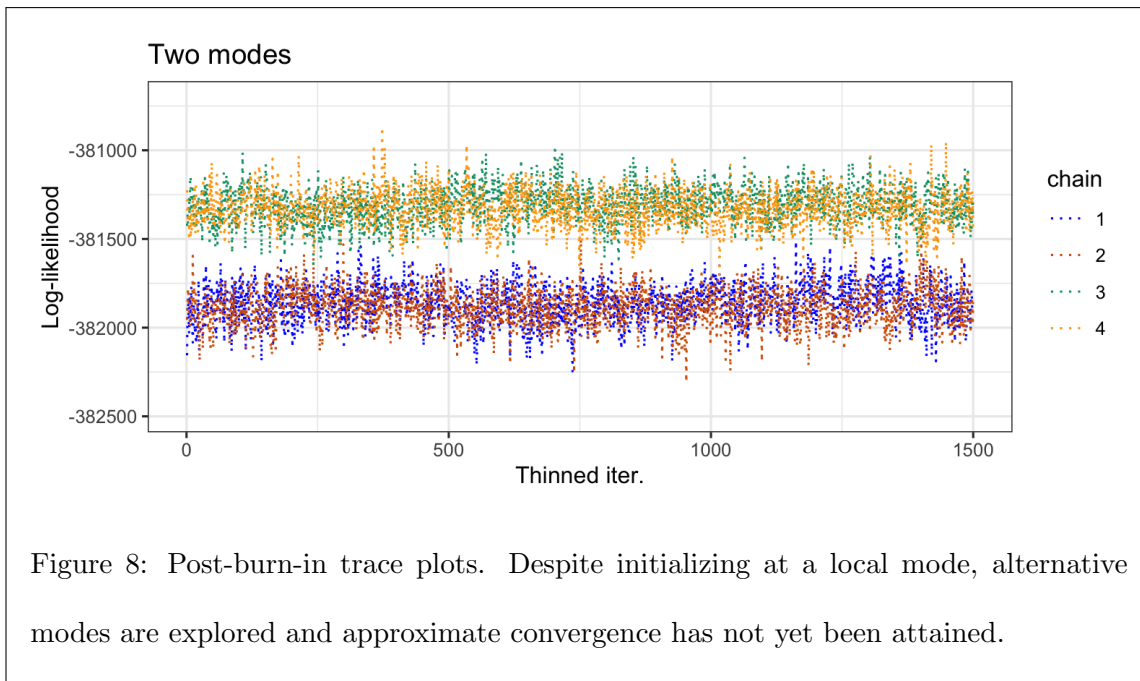
B Computation details

Our product formulation of factors $(c_{il}\phi_{il})$ and loadings $(s_{jl}\gamma_{jl})$ naturally facilitates Gibbs sampling, but a pseudo-prior analogous to those first introduced for variable selection by Dellaportas et al. (2002) is useful for tuning mixing properties. Our pseudo-prior is

$$(\gamma_{jl} \mid s_{jl} = 0, -) \sim \text{Ga}(1, \tau_0).$$

To further encourage exploration of the discrete latent space, we jointly update blocks of binary switches. At each iteration and for each $i = 1, \dots, n$ (resp. $j = 1, \dots, p$), factor indices $\{1, \dots, L\}$ are randomly partitioned into b blocks $\{l\}_b$ of size n_b . Switches within each block $\{c_{il} : l \in \{l\}_b\}$ ($\{s_{jl} : l \in \{l\}_b\}$) are jointly updated by drawing a configuration from the set of 2^{n_b} configurations. This is made simpler by the fact that posterior probabilities of candidate configurations are trivial to compute, and some configurations can be automatically rejected. A candidate $\hat{\mathbf{c}}_i$ ($\hat{\mathbf{s}}_j$) induces $\{\hat{\mu}_{i1}, \dots, \hat{\mu}_{ip}\}$ ($\{\hat{\mu}_{1j}, \dots, \hat{\mu}_{nj}\}$). If any $y_{ij} > 0$ such that $\hat{\mu}_{ij} = 0$, the candidate can be excluded from consideration, as $\Pr(y_{ij} > 0 \mid \mu_{ij} = 0) = 0$.

Poisson factorization models commonly exhibit multimodality beyond trivial nonidentifiability due to symmetry with respect to the order of factors and factor/loading scale ambiguity. Empirically, we find that several non-equivalent configurations of latent variables separated by regions of low probability can reasonably explain the data, and in large data settings, random initialization can result in slow or misleading mixing: multiple chains may explore the same mode for long periods before one discovers a region of higher probability, and if terminated prior to this discovery, MCMC diagnostics will indicate no issues.



This issue is more pronounced when many factors are used. Our objective in this study is to find the scientifically meaningful configuration or configurations of factors that *best* explain abundance, rather than exhaustively exploring all modes and characterizing uncertainty therein. Thus, as a practical remedy, we initialize each chain at the approximate maximum likelihood estimate prior to the burn-in period using the NMF R package (Gaujoux and Seoighe, 2010). We rescale the MLE so that $\sum_i \phi_{il} \approx 1$, and set $\mathbf{C} = \mathbf{1}_n \mathbf{1}_L^\top$ and $\mathbf{S} = \mathbf{1}_p \mathbf{1}_L^\top$. A warm start does not necessarily ensure good mixing, nor is the sampler trapped in the starting mode. For example, we fit a spatial-only model with 10 factors to the case study data; we use NMF initialization, 15,000 burn-in samples, and 15,000 samples (thinned by 10). Trace plots of the log-likelihood are shown in Figure 8; two distinct modes are represented by the four chains indicating the need for further sampling.

C MCMC diagnostics

Here, we present diagnostics for the models presented in Section 4. Generally, the concurrent ordination model requires more post-burn-in samples due to autocorrelation in latent

Model (L)	ℓ	$C \odot \Phi$	$S \odot \Gamma$	B	Ξ
Concuurent (6)	1.000	(0.999, 1.020)*	(0.999, 1.019)	(1.000, 1.021)	(0.999, 1.015)
Unconstrained (8)	1.001	(0.999, 1.021)**	(0.999, 1.041)	—	(0.999, 1.026)

Table 1: Potential scale reduction factors (PSRF) for log-likelihood (ℓ) and maximum/minimum elementwise PSRF for model parameters. *Approximately 15% (**1.5%) of factor switches c_{il} are equal to zero with probability $< 1/6000$ *a posteriori*, so PSRF is undefined; the reported range reflects convergence diagnostic statistics for those (i, l) which have nonzero posterior expected value.

regression coefficients B , whereas unconstrained or spatial ordination with more factors requires more burn-in samples to arrive at a common mode. To fit the concurrent model, we run the Gibbs sampler using four parallel chains for 100,000 iterations each; the first 25,000 samples are discarded as warm-up/burn-in. Following the burn-in, we retain every 50th sample to respect memory limits. The unconstrained model used to generate maps is also run for 100,000 iterations with 70,000 discarded and the remaining samples thinned by 20. The posterior summaries presented in Section 4 and the diagnostics presented here (Table 1) for the concurrent and spatial model are based on 6000 posterior samples. As noted in Supplement B, chains are not initialized at dispersed locations. However, the potential scale reduction factor diagnostic statistic (Gelman and Rubin, 1992) remains useful to confirm that all chains are exploring the same region.